Pérez-López, D.; Gasulla Mestre, I.; Capmany Francoy, J.; Sanchez Fandiño, JA.; Muñoz Muñoz, P.; Alavi, H. (2016). Third-order linearization for self-beating filtered microwave photonic systems using a dual parallel Mach-Zehnder modulator. Optics Express. 24(18):20632-20640. doi:10.1364/OE.24.020632.

Third-order linearization for self-beating filtered microwave photonic systems using a Dual Parallel Mach-Zehnder modulator

DANIEL PÉREZ,[1] IVANA GASULLA,[1] JOSÉ CAPMANY,[1,*] JAVIER S. FANDIÑO,[1] PASCUAL MUÑOZ,[1] AND HOSSEIN ALAVI[2]

[1] *ITEAM Research Institute, Universitat Politècnica de València, Camino de Vera, 46022 Valencia, Spain*
[2] *Intel Labs, Hillsboro, OR, USA*
* *jcapmany@iteam.upv.es*

Abstract: We develop, analyze and apply a linearization technique based on dual parallel Mach-Zehnder modulator to self-beating Microwave Photonics systems. The approach enables broadband low-distortion transmission and reception at expense of a moderate electrical power penalty yielding a small optical power penalty (<1 dB).

OCIS Codes: (060.2360) Fiber optics links and subsystems; (060.5625) Radio frequency photonics; (130.0250) Optoelectronics; (350.4010) Microwaves; (130.3120) Integrated optics devices.

References and Links

1. J. Capmany and D. Novak, "Microwave photonics combines two worlds," Nat. Photonics **1**, 316-330 (2007).
2. J. Yao, "Microwave photonics," J. Lightwave Technol. **27**(3), 314-335 (2009).
3. J. E. Mitchell, "Integrated wireless backhaul over optical access networks," J. Lightwave Technol. **32**(20), 3373-3382 (2014).
4. D. Pastor, B. Ortega, J. Capmany, P.Y. Fonjallaz, and M. Popov, "Tunable microwave photonic filter for noise and interference suppression in UMTS base stations," Electron. Lett. **40**, 997-999 (2004)
5. See "Technology focus on microwave photonics," Nat. Photonics **5**, 723–736 (2011).
6. A. L. Ricchiuti, J. Hervas, D. Barrera, S. Sales, and J. Capmany, "Microwave photonics filtering technique for interrogating a very-weak fiber bragg grating cascade sensor," IEEE Photonics J. **6**(6), 1-10 (2014).
7. D. A. I. Marpaung, C. Roeloffzen, R. Heideman, A. Leinse, S. Sales, and J. Capmany, "Integrated microwave photonics," Laser Photon. Rev. **7**, 506-538 (2013).
8. S. Iezekiel, M. Burla, J. Klamkin, D. Marpaung and J. Capmany, "RF engineering meets optoelectronics," IEEE Microwave Magazine **16**(8), 28-45 (2015).
9. W. Liu, M. Li, R. S. Guzzon, E. J. Norberg, J. S. Parker, M. Lu, L. A. Coldren, and J. P. Yao, "A fully reconfigurable photonic integrated signal processor," Nat.Photonics **10**, 190-195 (2016).
10. M. Li, Y. Deng , J. Tang , S. Sun , J. Yao , J. Azaña, N. H. Zhu, "Reconfigurable optical signal processing based on a distributed feedback semiconductor optical amplifier,"" Sci. Reports **6**, 19985 (2016)
11. D. Pérez, I. Gasulla, J. Capmany, J. S. Fandiño, P.Muñoz, and H. Alavi, "Figures of merit for self-beating filtered microwave photonic systems," Opt. Express **24**, 10087-10102 (2016).
12. C. H. Cox, III, *Analog Optical Links: Theory and Practice* (Cambridge University,) 2004.
13. S. K. Korotky and R. M. de Ridder, "Dual parallel modulation schemes for low-distortion analog optical transmission," IEEE J. Sel. Area Comm. **8**(7), 1377-1381 (1990).
14. H. Yamazaki, H. Takahashi, T. Goh, Y. Hashizume, T. Yamada, S. Mino, H. Kawakami, and Y. Miyamoto, "Optical modulator with a near-linear field response," J. Lightwave Technol. **34** (2016, in press).
15. M. Hochberg and L. Chrostowski *Silicon Photonics Design: From Devices to Systems* (Cambridge University,) 2015.

1. Introduction

Microwave photonics (MWP) [1,2], is expected to extend its use in the next years to novel emerging information technology scenarios, such as in mobile communications [3,4], data transmission [5] and sensing [6], which require technical approaches capable of smoothly interfacing the wireless and fibre network segments. MWP is the best positioned technology to achieve this target provided that it can enable agile and reconfigurable subsystems, featuring broadband operation and low space, weight and power (SWaP) metrics. Resorting to integrated microwave photonics [7,8], where complex MWP systems are integrated on a single chip [9,10], is the most promising approach to achieve the former targets. Furthermore,

it is highly desirable to evolve from pure intensity modulated and direct detection configurations to self-coherent detection schemes [11] allowing for advanced modulation formats.

Together with radiofrequency Gain and Noise Figure, one of the main factors that must be addressed by these systems is their linearity [12]. This is especially important in wireless communication technologies where the proliferation of carriers in the available spectrum, together with an increase in modulation bandwidths, exacerbate the presence and strength of these unwanted terms falling within allocated frequency bands, reducing the receiver carrier-to-noise ratio and the spurious free dynamic range. In most MWP systems, the main source of intermodulation and harmonic distortion is due to the nonlinear modulation characteristic of Mach-Zehnder modulators (MZM). This topic has been well studied and various electronic and optical techniques have been proposed over the years [12]. A technique that is particularly interesting for integrated configurations is based on a combination of MZM devices in parallel [13], where the modulator internal parameters are carefully designed so a destructive interference photocurrent is obtained for a target intermodulation order, improving the system linearity as compared to the configuration using a single modulator. These techniques, however, were proposed for direct detection and, therefore, there is no evidence reported so far on whether they can be appropriate for self-beating coherent systems. As recently outlined [14], this remains still an open question.

In this paper, we propose the use of a Dual Parallel Mach-Zehnder Modulator (DPMZM) for the linearization of self-beating coherent MWP systems. Taking as a start point the work developed in [11], we derive a full end-to-end systems model in section 2 that renders both the fundamental as well as the second- (IMD2) and third- (IMD3) order intermodulation distortion terms. In section 3, we specialize this model to derive the conditions leading to the suppression of the third-order intermodulation, finding two simple design cases for which IMD3 is suppressed with a very low penalty on the fundamental tone current. Furthermore, IMD2 is also mitigated as compared to the case where no linearization technique is employed. We provide a discussion and a comparison of the results obtained using the two cases as well. Furthermore, we compare our approach with that based on a recently proposed near linear field response modulator (NLFRM) recently reported [14]. Finally, section 4 provides some conclusions and future directions of research.

2. General model for amplitude modulation and single detection

Figure 1 shows the layout of a general self-beating filtered MWP system based in self-homodyne coherent detection with amplitude modulation described in [11], where the modulation stage incorporates a DPMZM to perform the linearization process. The rest of the system parameters are defined in [11]. Similarly to the technique developed in [13] for direct detection systems using two parallel MZMs, we have derived an analytical end-to-end model exploiting the same physical principle of achieving destructive interference in the detected photocurrent for a desired intermodulation order and maximizing the fundamental term relation, providing the optimum parameters of the modulator to suppress the IMD3.

We have followed similar steps as those described in [11], to obtain the photocurrent associated with the self-beating term for both the fundamental and the intermodulation tones. As a result, there are seven degrees of freedom for the linearized system design: the two bias voltages of the MZMs defined by $\phi_{dc,i} = \pi V_{dc,i}/V_\pi$, the excess coupling ratio γ of the (same) RF signal supplied to one of the modulators with respect to the other, where $\phi_{rf,1} = \pi V_{rf}/V_\pi$ and $\phi_{rf,2} = \gamma\phi_{rf,1}$, the optical in- and out- coupling ratios in the DPMZM (a and b, respectively) and the phase shifts for the upper and the lower arms (ψ_1 and ψ_2). In particular, the physical meaning of $\gamma > 1$ is related to the increase in the RF amplitude voltage that has to be applied to one modulator with respect to the value applied to the other and therefore, can be considered as an electrical power penalty $EP = 20 \log(\gamma)$.

By developing the same analytical procedure used in [11], but including the DPMZM, the fundamental tone C at the frequency $\Omega_1$is given by the photocurrent beating term $\widehat{I_b}(\omega_1)$:

$$C(\omega_1)=\widehat{I_b}(\omega_1)=-I_{dc}\sqrt{a_U a_L}CD\left(\frac{f_{RF1}}{4}\right)\left[\sqrt{(1-a)(1-b)}\sin(f_{DC1})A^{I,B}_{1,\omega_1}+g\sqrt{ab}\sin(f_{DC2})A^{I,B}_{2,\omega_1}\right], \quad (1)$$

where

$$A^{I,B}_{i,\Omega_1}=\cos\varphi\frac{\left[H_i(\omega_o+\Omega_1)-H_i^*(\omega_o-\Omega_1)\right]}{\sin\left(\frac{\phi_{DCi}}{2}\right)}, \quad (2)$$

$$H_i(\omega)=H(\omega)e^{j\psi_1}.$$

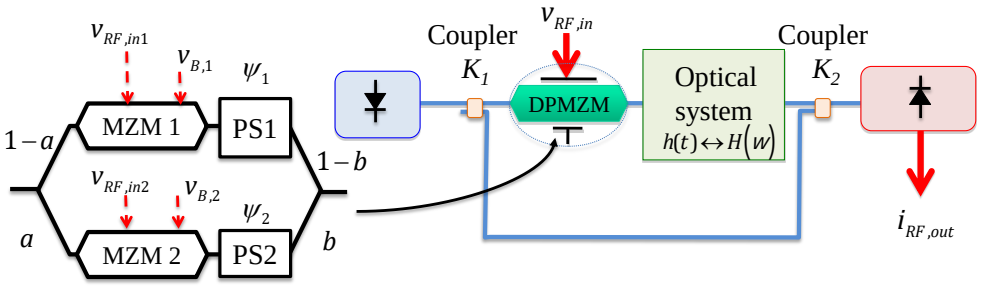

Fig. 1. (Left) DPMZM scheme and (Right) self-homodyne MWP system architecture.

The second-order intermodulation component IMD2 at frequency (Ω_1- Ω_2) is given by the photocurrent beating term $\widehat{I_b}(\omega_1-\omega_2)$:

$$IMD2(\omega_1-\omega_2)=\widehat{I_b}(\omega_1-\omega_2)=-jI_{dc}\sqrt{a_U a_L}CD\left(\frac{f_{RF}}{4}\right)^2\left[\sqrt{(1-a)(1-b)}A^{I,B}_{1,\omega_1-\omega_2}+g^2\sqrt{ab}A^{I,B}_{2,\omega_1-\omega_2}\right], \quad (3)$$

where

$$A^{I,B}_{i,\Omega_1-\Omega_2}=2\left[H_i(\omega_o+\Omega_1-\Omega_2)-H_i^*(\omega_o-\Omega_1+\Omega_2)\right]\sin(\phi_{DCi}/2)\cos\varphi, \quad (4)$$

And finally, the third-order intermodulation component IMD3 at frequency ($2\Omega_1$- Ω_2) is given by the photocurrent associated to the beating term $\widehat{I_b}(2\omega_1-\omega_2)$:

$$IMD3(2\omega_1-\omega_2)=\widehat{I_b}(2\omega_1-\omega_2)=-I_{dc}CD\sqrt{a_U a_L}\left(\frac{f_{RF}}{4}\right)^3\left[\begin{matrix}\sin(f_{dc1})\sqrt{(1-a)(1-b)}A^{I,B}_{1,2\omega_1-\omega_2}\\+g^3\sin(f_{dc2})\sqrt{ab}A^{I,B}_{2,2\omega_1-\omega_2}\end{matrix}\right], \quad (5)$$

where

$$A^{I,B}_{i,2\Omega_1-\Omega_2}=\frac{\left[H_i(\omega_o+2\Omega_1-\Omega_2)-H_i^*(\omega_o-2\Omega_1+\Omega_2)\right]}{2\sin(\phi_{dci}/2)}\cos\varphi. \quad (6)$$

3. Third-order intermodulation distortion linearization

We understand here the third-order linearization as the process of finding a value of γ that cancels the IMD3 photocurrent (Eq. (5)) maximizing at the same time the fundamental photocurrent term without increasing the second-order intermodulation IMD2 photocurrent. By forcing Eq. (5) to zero and solving for γ, we obtain the optimum value as:

$$\gamma=\sqrt[3]{-\sqrt{\frac{(1-a)(1-b)}{ab}}\left[\frac{H(\omega_o+2\Omega_1-\Omega_2)e^{j\psi_1}-H^*(\omega_o-2\Omega_1+\Omega_2)e^{-j\psi_1}}{H(\omega_o+2\Omega_1-\Omega_2)e^{j\psi_2}-H^*(\omega_o-2\Omega_1+\Omega_2)e^{-j\psi_2}}\right]\frac{\cos(\phi_{dc1}/2)}{\cos(\phi_{dc2}/2)}}. \quad (7)$$

In practice, we prefer a real value of γ since otherwise an extra RF phase shifter has to be inserted prior to the RF modulation input of one of the MZMs. A real value for γ is obtained if $\psi_1 = \pi$ and $\psi_2 = 0$:

$$\gamma = \sqrt[3]{\sqrt{\frac{(1-a)(1-b)}{ab}}\frac{\cos(\phi_{dc1}/2)}{\cos(\phi_{dc2}/2)}}. \tag{8}$$

For comparison purposes, it is necessary to know in which way the fundamental and the IMD2 terms are affected by the linearization process. Ideally, the photocurrent associated to the linearized fundamental tone C_L should not decrease whereas the $IMD2_L$ should do. Fig. 2 (a) shows the spectral components where one MZI is employed without linearization, i.e. $a = b = 0$, $\gamma = 0$, while Fig. 2(b) shows the spectral components after the linearization process that employs the DPMZM. As a figure of merit to evaluate the change produced in the fundamental and the IMD2 contributions by the linearization process, we define the ratio between the linearized and unlinearized second order intermodulation terms $IMD2_L$/ IMD2 and the ratio between the linearized and unlinearized fundamental terms C_L/ C as:

$$\frac{CIMD2_L}{CIMD2} = \frac{C_L/IMD2_L}{C/IMD2} = \frac{\widehat{I_{b,L}}(W_1)/\widehat{I_{b,L}}(W_1 - W_2)}{\widehat{I_b}(W_1)/\widehat{I_b}(W_1 - W_2)}. \tag{9}$$

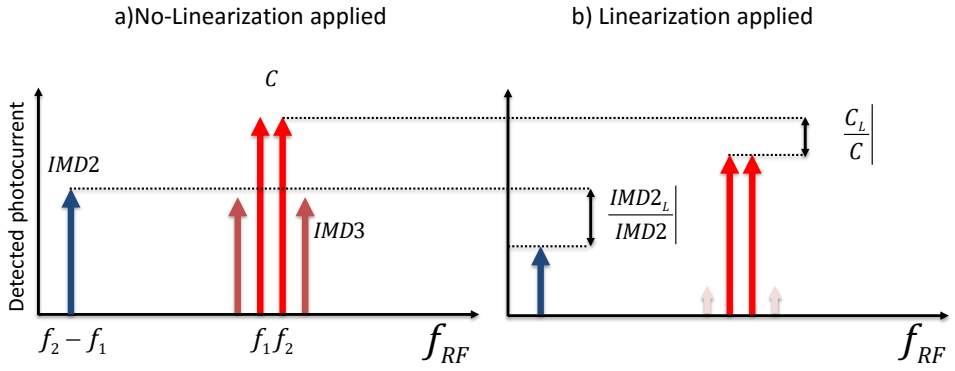

Fig. 2. Photodetected spectrum without (Left) and with the applied linearization (Right)

We require values greater than 1 for this figure of merit to guarantee that the second-order distortion compared to the fundamental term is not increased as a result of the IMD3 suppression. We have identified two cases of practical interest due to their simplicity in terms of the required values for the bias points and phase shifters in the two arms of the DPMZM.

3.1 Case 1: $\psi_1 = \pi$ and $\psi_2 = 0$, $\varphi_{dc,1} = \varphi_{dc,2} = \pi/2$

In this case, our degrees of freedom in the DPMZM are the coupling constants (a and b) of its in- and out- Y junctions, which we can actually design, optimize and fix. Both upper- and lower- arm modulators are biased in quadrature and will modulate the same RF signal. However, as previously mentioned, the lower modulator will be feed with the same RF signal as the upper modulator but with a voltage amplitude excess given by $\gamma = \varphi_{RF2}/\varphi_{RF1}$. Finally, there is a static π-phase shift between the upper and lower arms of the DPMZM to produce destructive interference between the parallel outputs. By substituting the parameters values, we can directly obtain from Eq. (8) the necessary value of γ to suppress the IMD3:

$$\sqrt{(1-a)(1-b)} - g^3\sqrt{ab} = 0 \tag{10}$$

The ratio between linearized and unlinearized ($a = b = 0$) fundamental tone currents C_L/C is obtained from Eq. (1):

$$\frac{C_L}{C} = \sqrt{(1-a)(1-b)} - g\sqrt{ab} \tag{11}$$

and must be maximized subject to the condition given by Eq. (10). This is done by means of a Lagrange multipliers method, which is described in detail in the appendix. The outcome of this optimization renders the following values for a and b:

$$a = b = \frac{1}{1+\gamma^3}. \tag{12}$$

Under this condition, the ratios between the linearized photocurrents and the unlinearized terms are obtained as:

$$\left.\frac{C_L}{C}\right|_{MAX} = \frac{g(g^2-1)}{1+g^3}; \tag{13}$$

$$\frac{IMD2_L}{IMD2} = \frac{\widetilde{I_L}(W_1 - W_2)}{\widetilde{I}(W_1 - W_2)} = \frac{g^2(g-1)}{1+g^3}. \tag{14}$$

Substituting Eqs. (13) and (14) in Eq. (9), we have:

$$\frac{CIMD2_L}{CIMD2} = 1 + \frac{1}{\gamma}. \tag{15}$$

Figure 3 (upper left) shows the results computed for Eqs. (13)-(15) against the electrical power penalty $EP = 20 \log(\gamma)$, [13]. As far as the fundamental current is concerned, the black trace indicates that, in principle, almost negligible optical penalty can be achieved in theory provided that an electrical penalty of over 10 dB can be assumed. In practical terms, and due to the coupling of the electrical penalty with the values of the optimized splitting ratios for the input and output Y branches of the DPMZM, (Eq. (12)), there is a maximum electrical penalty that can be assumed if realistic splitting ratios are to be employed. This is illustrated in the lower left part of Fig. 3, where we plot Eq. (12) versus *EP*. If, for instance, a minimum value o*f* $a = 0.05$ can be assumed due to fabrication tolerances, the maximum affordable electrical penalty is around 9 dB, which results in an optical penalty slightly below 1 dB. In a similar way, the blue trace curve describes the system's behavior as related to IMD2. The first interesting feature is that, for any value of the electrical penalty, the blue curve remains above the black curve. This means that upon this third-order linearization process the IMD2 photocurrent always suffers a higher attenuation than that of the fundamental tone. The solid red line indicates that, at the same time that IMD3 is suppressed, the IMD2 term experiences a greater attenuation as compared to that experienced by the fundamental tone. This means that as far as IMD2 is concerned, the system linearity is also improved.

3.2 Case 2: $\psi_1 = \pi$ and $\psi_2 = 0$, $\varphi_{dc,1} = \varphi_{dc,2} = \pi/2$, $b = 1/2$

This is a particular condition of Case 1, where b is fixed to ½ to obtain two balanced modulated outputs. Since now there is one variable less than in Eq. (11), we obtain a direct relation that yields the optimum operation:

$$a = \frac{1}{1+\gamma^6}; \tag{16}$$

$$\left.\frac{C_L}{C}\right|_{\max} = \frac{g\left(g^2 - 1\right)}{\sqrt{2\left(1+g^6\right)}}. \tag{17}$$

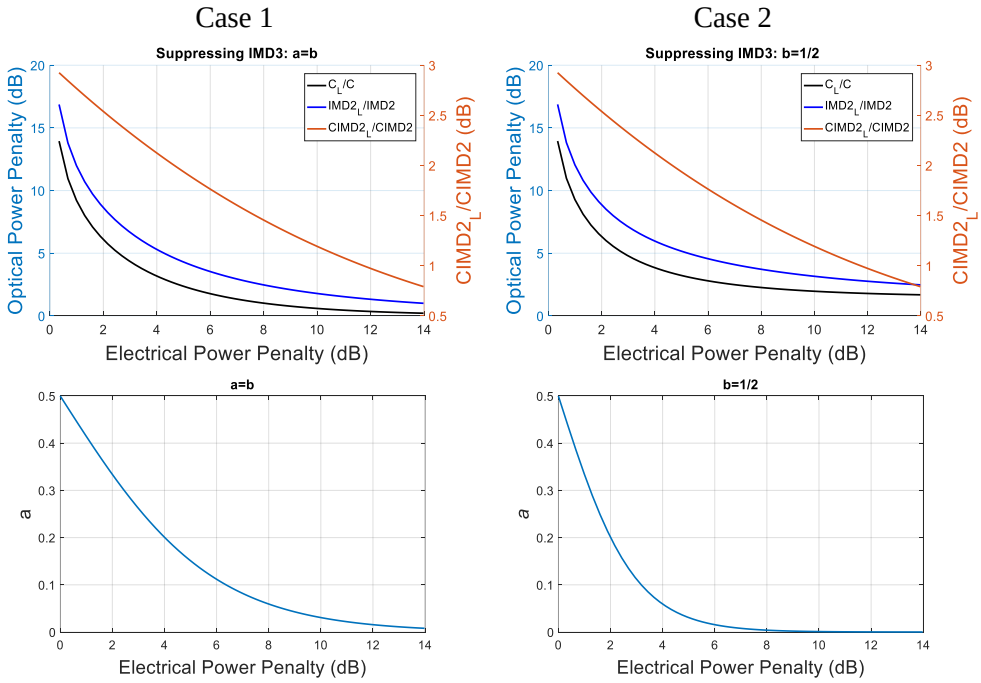

Fig. 3. Case 1. (Upper) Optical penalties vs Electrical Penalties, (Lower) Coupler coefficient vs Electrical Penalty for Case 1 (left) and Case 2 (right).

$$\frac{IMD2_L}{IMD2} = \frac{\gamma^2\left(\gamma - 1\right)}{\sqrt{2\left(1+\gamma^6\right)}}. \tag{18}$$

Substituting Eqs. (17) and (18) in Eq. (9), we obtain exactly the same value given by Eq. (15). The right part of Fig. 3 shows the results for this case, where we observe a similar behavior as in case 1. However, the range of allowed electrical penalty values is reduced (5 dB as compared to 8 dB of case 1), while the minimum optical penalty for the fundamental tone is increased of (around 4.5 dB as compared to 1 dB of case 1). As in case 1, the behavior as compared to IMD2 is improved and, in fact, the relative improvement is the same in both equalization methods.

3.3 Discussion

Both linearization cases are in principle capable of cancelling third-order intermodulation distortion from the modulation stage while, at the same time, improving the linearity of the system as related to second-order intermodulation distortion. Note that whereas the standard/commercial DPMZMs are usually symmetric it is feasible to obtain asymmetric coupling in Y-branches by proper design [15]. In the first case, a better performance is obtained in terms of optical power penalty for the fundamental tone (i.e. smaller than in case 2 for the same amount of electrical power penalty). This is achieved at the expense of a more complex design of the DPMZM since both the input and output Y-branch splitting ratios are asymmetric. However, as a result from the optimization process, both have the same value (Eq. (12)). In case 2, one of the two Y-branches can be symmetric, however this does not render any significant advantage in terms of fabrication. Since case 2 is more restrictive in terms of affordable electrical power penalty the conclusion is that the approach of case 1 is

preferable from the practical point of view. Note however that the optimum bias point for IMD3 suppression should be kept fixed and this requires the stabilization of the bias voltages for the upper and lower MZMs as well as for the phase shifters to avoid the drifting of the optimum operation conditions.

It should be pointed out as well that none of the two cases can obtain simultaneous cancellation of second- and third-order intermodulation distortion despite that fact that both MZMs at the two DPMZMs are biased in quadrature. This is not surprising as second-order intermodulation distortion cancellation at quadrature biasing points is only achieved for the case of direct detection, that is for intensity modulators, while the system under consideration here works under self-beating coherent detection, that is for electric field modulators. In fact, the topic of linearized electric field modulators has been scarcely addressed in the literature but is currently rising interest as coherent systems are becoming commonplace in optical fiber communications. A possible configuration for a near linear field response modulator (NLFRM) has been reported very recently in [14], which proposes a two-stage modulator configuration as shown in Fig. 4.

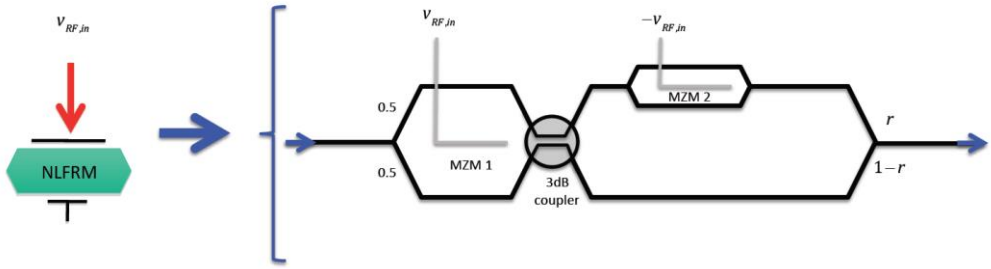

Fig. 4. Configuration for a Near-linear Field Response modulator reported in [12].

The layout includes two MZMs, just as in the case of the DPMZM, so the overall device complexity is similar. The difference here is that the modulators are placed in tandem and there are two separate paths for signal propagation. One path traverses two modulators in series while the second one only propagates through one modulator. The two stages are connected by a 2x2, 3-dB coupler. The Y-branch at the left is a 3-dB configuration while the one closing the right part is asymmetric and has a power ratio given by *r*. Another difference with the DPMZM configuration resides in the fact that the same RF input voltage (but opposed in phase) is employed to drive the two modulators (i.e., there is no RF power penalty γ).

In particular, the output-input field relationship in the modulator of Fig. 4 is given by:

$$E_{out,\mathrm{modulator}} = E_{in}\left[\sqrt{1-r}\sin\left(\frac{\phi_{RF}}{2}\right)-\frac{\sqrt{r}}{2}\sin\left(\phi_{RF}\right)\right]= \\ =\frac{E_{in,\mathrm{modulator}}}{2j}\left\{\sqrt{1-r}\left[e^{j\frac{\phi_{RF}}{2}}-e^{-j\frac{\phi_{RF}}{2}}\right]-\frac{\sqrt{r}}{2}\left[e^{j\phi_{RF}}-e^{-j\phi_{RF}}\right]\right\}, \tag{19}$$

where $\Phi_{RF} = \pi\ V_{RF}/V_{\pi}$. Using Eq. (19), we can follow a similar process here to derive the output photocurrents for the fundamental, second- and third-order intermodulation tones when the MZM device in the self-beating MWP link is replaced by the NLFRM in the system of Fig. 1. We can then compare both approaches. For the fundamental tone we have:

$$\hat{I}_{bL}\left(\omega_1\right) \approx j2I_{dc}\sqrt{a_U a_L}CD\left[\sqrt{1-r}\left(\frac{f_{RF}}{4}\right) - \frac{\sqrt{r}}{2}\left(\frac{f_{RF}}{2}\right)\right]A^{I,B}_{\omega_1},$$
$$A^{I,B}_{\omega_1} = \left\{H\left[\omega_o + \omega_1\right] + H^*\left[\omega_o - \omega_1\right]\right\}\cos\varphi\,. \tag{20}$$

The IMD2 contribution is:

$$\hat{I}\left(\omega_1 - \omega_2\right) = j2I_{dc}\sqrt{a_U a_L}CD\left\{\begin{matrix} B_{1,-1}H\left[\omega_o + n\omega_1 + k\omega_2\right]e^{j\left(\omega_o + n\omega_1 + k\omega_2\right)t} - \\ - B^*_{-1,1}H^*\left[\omega_o + n\omega_1 + k\omega_2\right]e^{-j\left(\omega_o + n\omega_1 + k\omega_2\right)t}\end{matrix}\right\}\cos\varphi = \tag{21}$$
$$= \left\{B_{1,-1} = B_{-1,1} = 0\right\} = 0,$$

not surprisingly, it is completely suppressed as the modulator response is linearized to cancel even order intermodulation distortions. Finally, the IMD3 contribution is:

$$\hat{I}\left(2\omega_1 - \omega_2\right) = -jI_{dc}CD\sqrt{a_U a_L}CD\left[\sqrt{1-r}\left(\frac{f_{RF}}{4}\right)^3 - \frac{\sqrt{r}}{2}\left(\frac{f_{RF}}{2}\right)^3\right]A^{I,B}_{2\omega_1-\omega_1}, \tag{22}$$
$$A^{I,B}_{2\omega_1-\omega_1} = \left\{H\left[\omega_o + 2\omega_1 - \omega_2\right] + H^*\left[\omega_o - 2\omega_1 + \omega_2\right]\right\}\cos\varphi\,.$$

To linearize the overall response, the photocurrent of the IMD3 term must cancel and therefore:

$$\hat{I}\left(2\omega_1 - \omega_2\right) = 0 \Rightarrow \sqrt{1-r}\left(\frac{f_{RF}}{4}\right)^3 - \frac{\sqrt{r}}{2}\left(\frac{f_{RF}}{2}\right)^3 = 0, \tag{23}$$
$$\frac{\sqrt{1-r}}{64} = \frac{\sqrt{r}}{16} \Rightarrow 1 - r = 16r \Rightarrow r = \frac{1}{17} \approx 0.06$$

and this leads to a fundamental tone photocurrent given by:

$$\hat{I}_{bL}\left(\omega_1\right) \approx jI_{dc}\sqrt{a_U a_L}CD\left(\frac{f_{RF}}{2}\right)\left[\sqrt{\frac{16}{17}} - \sqrt{\frac{1}{17}}\right]A^{I,B}_{\omega_1} =$$
$$= j0.364I_{dc}\sqrt{a_U a_L}CDf_{RF}A^{I,B}_{\omega_1}, \tag{24}$$
$$A^{I,B}_{\omega_1} = \left\{H\left[\omega_o + \omega_1\right] + H^*\left[\omega_o - \omega_1\right]\right\}\cos\varphi\,.$$

If we compare this value to that obtained when no linearized modulator is employed (Eq. (19) subject to the condition r=0), we finally find:

$$\frac{\hat{I}_{bL}\left(\omega_1\right)}{\hat{I}_b\left(\omega_1\right)} = 0.728. \tag{25}$$

Therefore, the photocurrent of the fundamental tone when linearization is employed is reduced by a 27% or the RF power by a 47%, in other words, roughly by 3 dB

4. Summary and conclusions

We have developed, analyzed and applied a linearization technique based on DPMZM in self-homodyne MWP systems. The approach enables broadband low-distortion transmission and reception at expense of an additional moderate electrical power penalty while yielding a low optical power penalty (<1 dB). Two practical linearization cases were identified. In the optimum case, non-symmetrical (but equal) signal division ratios at the input and output Y-branches of the DPMZM are required. In the second, the signal division ratio at the output Y-branch is symmetric (50%) while the input Y-branch division ratio is asymmetric. In both cases, IMD3 cancellation is accompanied with a reduction of the IMD2 values. For self-beating coherent detection, a complete and simultaneous cancellation of both IMD2 and IMD3 terms will require a near linear field response modulator, such as that reported in [14] and for which we have derived the fundamental, second- and third-order intermodulation distortion terms for the sake of comparison. While the NLFRM approach can achieve complete IMD2 and IMD3 cancellation, its optical penalty is 3 dB. In the DPMZM case, only IMD3 cancellation is achieved while IMD2 is suppressed with an optical penalty that can be as low as 1 dB.

Funding

This research work is funded by INTEL Corporation. The work of D. Pérez was supported by the FPI-UPV Grant Program from the Universitat Politècnica de València and the work of I. Gasulla was supported by the Spanish MINECO through the Ramón y Cajal Program.

Appendix

We aim to maximize Eq. (11) subject to the condition given by Eq. (10). The Lagrangian is thus given by:

$$L(a,b)=\sqrt{(1-a)(1-b)}-\gamma\sqrt{ab}+\lambda\left[\sqrt{(1-a)(1-b)}-\gamma^3\sqrt{ab}\right], \tag{26}$$

where λ is the Lagrange multiplier. We now compute:

$$\begin{aligned}
&\frac{\partial L}{\partial a}=-\frac{\sqrt{(1-b)}}{2\sqrt{(1-a)}}+\frac{\gamma\sqrt{b}}{2\sqrt{a}}+\lambda\left[\frac{\sqrt{(1-b)}}{2\sqrt{(1-a)}}+\frac{\gamma^3\sqrt{b}}{2\sqrt{a}}\right]=0,\\
&\frac{\partial L}{\partial b}=-\frac{\sqrt{(1-a)}}{2\sqrt{(1-b)}}+\frac{\gamma\sqrt{a}}{2\sqrt{b}}+\lambda\left[\frac{\sqrt{(1-a)}}{2\sqrt{(1-b)}}+\frac{\gamma^3\sqrt{a}}{2\sqrt{b}}\right]=0,\\
&\frac{\partial L}{\partial \lambda}=\sqrt{(1-a)(1-b)}-\gamma^3\sqrt{ab}=0.
\end{aligned} \tag{27}$$

The first equality in Eq. (26) leads to:

$$\frac{\partial L}{\partial a}=0\Rightarrow\lambda=\frac{-\sqrt{a(1-b)}+\gamma\sqrt{(1-a)b}}{\sqrt{a(1-b)}-\gamma^3\sqrt{(1-a)b}}. \tag{28}$$

The second equality in Eq. (26), taking into consideration Eq. (27), leads to:

$$\frac{\partial L}{\partial b}=0\Rightarrow\frac{1-a}{a}=\frac{1-b}{b}\Rightarrow a=b. \tag{29}$$

Finally, the third equality in Eq. (26) yields:

$$\frac{\partial L}{\partial \lambda} = 0 \Rightarrow (1-a) - \gamma^3 a = 0 \Rightarrow a = b = \frac{1}{1+\gamma^3}. \tag{30}$$